The Influence of Geometrical and Inlet Parameters on the Impingement Cooling of Aviation Kerosene

Yunfei Xing

State Key Laboratory of High Temperature Gas Dynamics,
Institute of Mechanics,
Chinese Academy of Sciences,
Beijing 100190, China

Wenhui Fan

State Key Laboratory of High Temperature Gas Dynamics,
Institute of Mechanics,
Chinese Academy of Sciences,
Beijing 100190, China;
School of Engineering Science,
University of Chinese Academy of Sciences,
Beijing 100049, China

Mengmeng Du

Science and Technology on Liquid Rocket Engine
Laboratory,
Xi'an Aerospace Propulsion Institute,
Xi'an 710100, China

Fengquan Zhong[1]

State Key Laboratory of High Temperature Gas Dynamics,
Institute of Mechanics,
Chinese Academy of Sciences,
Beijing 100190, China;
School of Engineering Science,
University of Chinese Academy of Sciences,
Beijing 100049, China
e-mail: fzhong@imech.ac.cn

In the present paper, numerical study of flow and heat transfer properties of RP-3 kerosene in an impingement model are conducted with SST $k - \omega$ turbulence model and a 10-species surrogate of kerosene. The independence of grids is first studied and the numerical results are compared with experimental data for validation. Characteristics of flow and heat transfer of kerosene flow in the impingement model are studied with different inlet temperatures, dimensionless open areas, and separation distances. The heat transfer coefficients and pressure losses increase with decreasing dimensionless open areas. The separation distance $H/d = 2$ gets the best heat transfer performance and the separation distance $H/d = 3$ gets the best heat transfer uniformity on the target plate. Higher inlet temperature gets a higher heat transfer performance and heat transfer uniformity on the target plate. [DOI: 10.1115/1.4054278]

Keywords: impingement cooling, heat transfer, kerosene, numerical study

1 Introduction

Active cooling using hydrocarbon fuels as coolant has been a widely used method for thermal protection of rocket and scramjet applications. To limit the weight of the cooling system, regenerative cooling using onboard fuel as the primary coolant is considered most effective. Flow and heat transfer properties of hydrocarbon fuels in circular or rectangular cooling channels have been studied via heating facility [1–3] or numerical simulations [4–6]. Many previous studies on the heat transfer of hydrocarbon fuels are focused on supercritical properties and fully developed pipe flows [4–7]. Extensive combustion and local structures always cause local peaks of heat flux for rocket or scramjet combustors. For example, for a Mach 2.5 supersonic combustor, local heat flux may reach 3–4 MW/m², which is at least three times the average wall heat flux [8]. The commonly used convective heat transfer of cooling channel flow is no longer able to absorb heat from the wall efficiently and keep the wall temperature within the safe range. Therefore, effective cooling concepts are required for these highly loaded components. Impinging jets, due to their ability to achieve high heat transfer rates, have been used in gas turbines cooling applications such as the cooling of turbine vanes and blades, and combustor liners [9–12].

Most of previous studies on impingement jet cooling are focused on gaseous or simple liquid jets. The density and viscosity of kerosene decrease remarkably in the vicinity of the critical point as functions of temperature and pressure, which has been proved by our previous study [6]. It is expected that flow and heat transfer properties of supercritical kerosene would exhibit unique characteristics due to significant changes in the thermodynamic and transport properties [6]. Xing et al. [13] investigated the impingement cooling of aviation kerosene at supercritical conditions numerically. It is found that the heat transfer rates are influenced by the inlet temperature apparently. For the scramjet application cooling, the inlet temperature of regenerative cooling system is increased due to the upstream heat transfer and there is a significant diffidence of heat transfer for aviation kerosene when the temperature is increased. Therefore, it is necessary to explore the impingement heat transfer performance with high inlet temperature.

2 Geometry of Impingement Configuration

Kerosene flow in an impingement model is studied numerically. The impingement model and impingement plate configuration are shown in Fig. 1. The flow enters the inlet plenum followed by the impinging jets generated by an impingement plate, and the flow exits the outlet plenum after impinging on the target wall. The inlet pressure is 5 MPa. The inlet mass flowrate is 20 g/s (mass flow rate has usually been used instead of Reynolds number as one of the key parameters for the cooling system).

In the present study, the diameter of the jets is 1 mm, the length of the plate (L_x) is 32 mm and the width of the plate (L_y) is 24 mm. In order to explore the influence of the impingement configuration, different jet arrangements are investigated. All geometric parameters are typically based on the diameter of the jets (d), which applies to the separation distance ($H/d = 1, 2, 3, 4$, and 5), the streamwise jet-to-jet distance ($S_x/d = 8, 12$, and 16), and the spanwise jet-to-jet spacing ($S_y/d = 8, 12$, and 24). Four different impingement plates are listed in Table 1. For information on the hole density of the jet system, the dimensionless open area A_f has been established as a characteristic parameter. It is defined as follows:

$$A_f = \frac{n \cdot \frac{\pi}{4} d^2}{L_x L_y}$$

Here, n is the jet number.

In the impingement system, we define a Reynolds number based on the jet diameter and jet velocity and ΔP is the pressure difference between inlet and outlet.

And the heat transfer coefficient h is defined as follows:
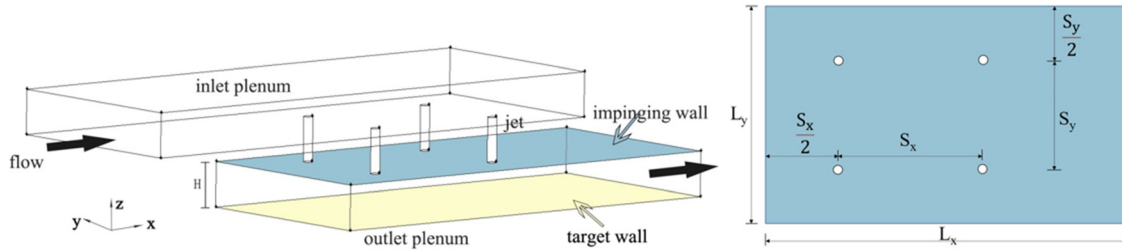
$$h = \frac{Q_w}{T_f - T_w}$$

Fig. 1 The sketch up of the impingement model

Table 1 The parameters of the impingement plate

Impingement plate	S_x/d	S_y/d	Jet number	A_f
	8	8	12	1.23%
B	12	12	6	0.61%
C	16	12	4	0.41%
D	16	24	2	0.21%

Table 2 Mesh parameters and grid independence results

Case	The height of the first grid (mm)	Averaged h	GCI (%)
a	0.01	11424	25.1%
b	0.005	11719	28.2%
c	0.001	11387	3.9%
d	0.0001	11414	0.4%

In order to analyze the local temperature distribution, the total averaged temperature on the target plate $\bar{T}_w$ and local temperature standard deviation σ are calculated as follows:

$$\bar{T}_w = \frac{1}{n}\sum_{i=1}^{n} T_{wi}$$

$$\sigma = \sqrt{\frac{1}{n}\sum_{i=1}^{n}\left(T_{wi} - \bar{T}_w\right)^2}$$

Here, T_f is the inlet temperature and T_w is the wall temperature on the target plate.

The ratio of local temperature standard deviation and the total averaged temperature on the target plate $\frac{\sigma}{\bar{T}_w}$ is used to evaluate the uniformity of the heat transfer distribution.

3 Numerical Method

The Reynolds-averaged Navier–Stokes equations are solved by finite volume method with 2nd-order upwind scheme applied for convective terms and 2nd-order central scheme for viscous terms. The SST k-ω turbulence model is applied to solve equations for simulating impingement jet impinging, which is proved effective for the simulation of impingement jet flows [14] and [15]. The SIMPLE algorithm is employed to resolve the coupling between velocity and pressure. The implicit Gauss–Seidel iteration is used to calculate the time advancement. An outflow boundary condition is applied to the outlet. The heat flux on the target wall is kept as $1\,\mathrm{MW/m^2}$, which is close to typical value of wall heat flux of a supersonic combustor [16]. A 10-species surrogate of aviation kerosene proposed in our previous study [6] is applied with the Extended Corresponding State (ECS) method to determine the thermophysical properties of kerosene such as density, specific heat, viscosity as functions of temperature and pressure.

3.1 Grid Independence.
A grid-independence study has been carried out for the validation of the present numerical method. Four meshes are studied. The total grids numbers are 70,000 (case a), 150,000 (case b), 300,000 (case c), and 500,000 (case d), respectively. We focus on the data on target plate, therefore the first layer mesh on the target plate is the only varied parameter here, as shown in Table 2. The results of grid-independence study are also reported in Table 2. The difference in heat transfer coefficient is less than 3% when the grids numbers are over 300,000. Besides, in order to evaluate the grid convergence of the solutions, the grid convergence index (GCI) [17] of those cases was calculated, and the results are shown in Table 2 as well. The results

indicate that the refinement of the grid is successful, and the simulation accuracy of Case c and Case d is much better. However, the computational time for Case d is nearly two times higher than that of Case c. Therefore, Case c is applied for all the simulations in the present study.

3.2 Comparison With Experimental Heat Transfer Data.
The experimental study is conducted under certain conditions and a detailed description about the experimental setup and the data analysis are given in our previous work [18]. The present numerical method is validated by comparison of calculated heat transfer coefficient on the target plate with experimental data. Figure 2 shows the normalized Nusselt number on the target plate with different inlet Reynolds number. The maximum difference of Nusselt number is 10.6%. The agreement between experimental and numerical values is very good. The numerical predicted values are higher than the measurement uncertainty (6.5%) slightly. The general modeling errors, such as the choice of boundary conditions or turbulence model and the discretization error may have contributed to the numerical errors. One can conclude that the numerical results are well consistent with the experimental results and the current numerical method is validated.
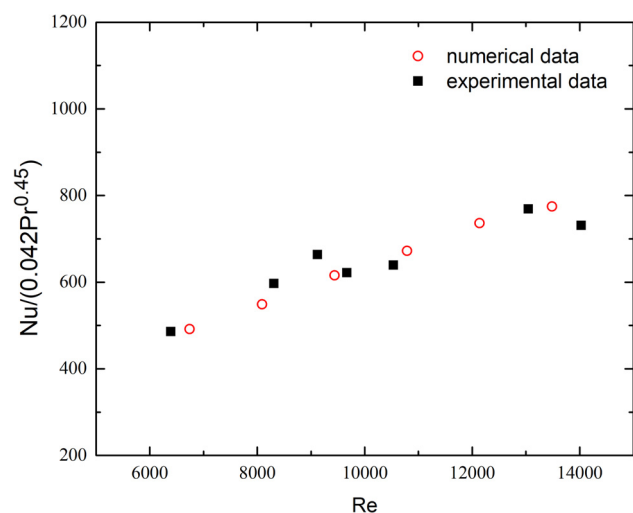

Fig. 2 Nusselt number comparison of the numerical and experimental data

Table 3 The heat transfer performance and pressure loss for different impingement plates ($H/d = 3$)

Impingement plate	Total averaged h (W/m^{2}K)	$\dfrac{\sigma}{\overline{T}_w}$	Pressure loss (kPa)
A	8666	9.3%	7
B	10887	8.7%	26
C	12600	7.7%	57
D	14386	10.9%	224

Table 4 The heat transfer performance and pressure loss for different inlet temperatures ($H/d = 3$)

Inlet temperature (K)	Jet velocity (m/s)	Total averaged h (W/m^{2}K)	$\dfrac{\sigma}{\overline{T}_w}$	Pressure loss (kPa)
300	8.2	8074.3	14.5%	47
500	10.5	12599.7	7.7%	57

4 Results and Discussions

4.1 The Influence of Impingement Plates. Figure 3 shows contours of heat transfer coefficient on the target plate with different impingement plates for the separation distance $H/d = 3$ and inlet temperature of 500 K. The positions of the impingement jets are clearly visible in the heat transfer pattern on the target plate. At the stagnation points, the heat transfer coefficient is highest due to the thin boundary layer. After the jets impinge on the target plate, heat transfer coefficients decrease quickly toward the sides. One can see that the heat transfer coefficients on the stagnation point are higher with fewer jet numbers caused by the higher inlet Reynolds number.

The impingement plate A gets the lowest total averaged heat transfer coefficient and the lowest pressure loss. The free jet region and wall jet region are not fully developed due to the relatively low Reynolds number of jets. The less interaction between adjacent jets causes the lower heat transfer performance. With the decreasing of the jet number, a higher overall heat transfer performance is obtained, as we can see in Table 3. The impingement plate D gets the highest total averaged heat transfer coefficient because of the higher heat transfer performance in the stagnation zone. While the lower impinging area also causes higher pressure loss compared with other impingement plates. Impingement plate C with the dimensionless open area 0.41% obtains a better uniform performance on the target plate. For the following discussion, the impingement plate C is only focused.

4.2 The Influence of Inlet Temperature. Table 4 lists the averaged heat transfer coefficients and pressure loss with impingement plate C for different inlet temperatures. One can see that the jet velocity increases with the increasing inlet temperature because the properties of kerosene change dramatically with the changing of inlet temperature. The higher impinging velocity causes better heat transfer performance on the target plate and relatively higher pressure loss. The higher inlet temperature obtains a better uniform performance on the target plate.

Figure 4 shows contours of heat transfer coefficient on the target plate with different impingement plates for the separation distance $H/d = 3$. One can see that the second peak of heat transfer coefficient occurs in the vicinity of the stagnation point of each kerosene jet, for inlet temperature of 500 K. The shifting of heat transfer peak with increased Reynolds number has been observed and discussed in the previous work with simple fluids such as air [19,20]. The shifting of heat transfer peak is caused by larger impingement jet velocity for higher inlet temperature.

4.3 Effect of Separation Distance (H/d). Figure 5 shows the local heat transfer coefficient distributions on the target plate and the turbulent kinetic energy of the jet flow. Large values of turbulent kinetic energy are found in the thin shear layer region on the target plate caused by the impingement jets and in the outer part of the impinging core. The increase in turbulent kinetic energy benefits the heat transfer performance. Multiple jet impingements can be thought of as a coupled effect of jet impingement and channel flow caused by the crossflow. The crossflow provides a significant direct contribution to the heat transfer coefficients in the downstream parts at a small separation distance. The velocity shear layer would enhance flow dynamics and generate significant vortices. For the separation distance $H/d = 1$, lower heat transfer coefficients are obtained because relatively narrow space restricts the development of jet wall flow.

The total averaged heat transfer coefficient and uniformity on the target plate is the lowest for the separation distance $H/d = 1\sim5$
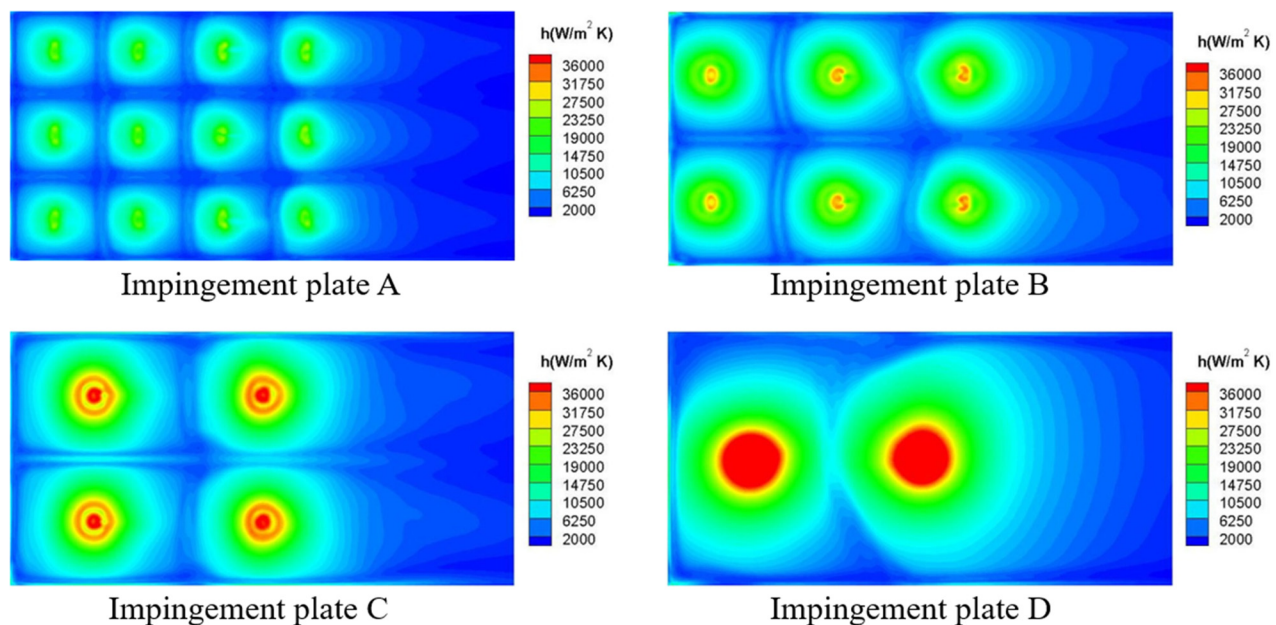

Impingement plate A

Impingement plate B

Impingement plate C

Impingement plate D

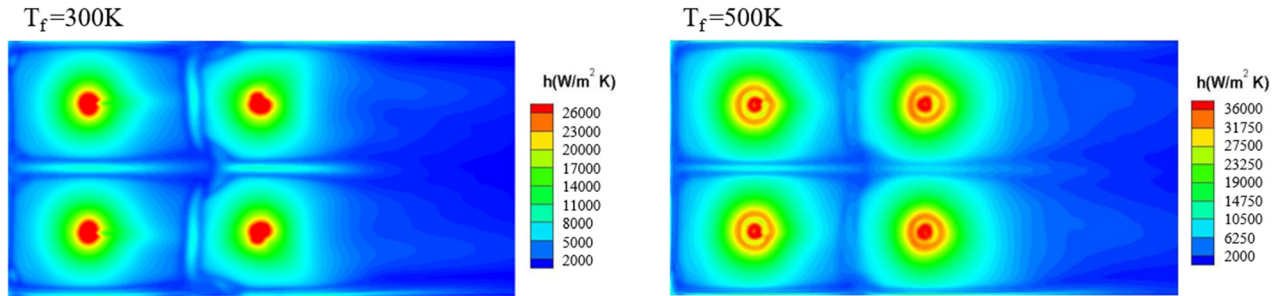**Fig. 3 Heat transfer coefficients distribution on the target plate ($H/d = 3$)**

Fig. 4 Heat transfer coefficients distribution on the target wall for different inlet temperature ($H/d = 3$)
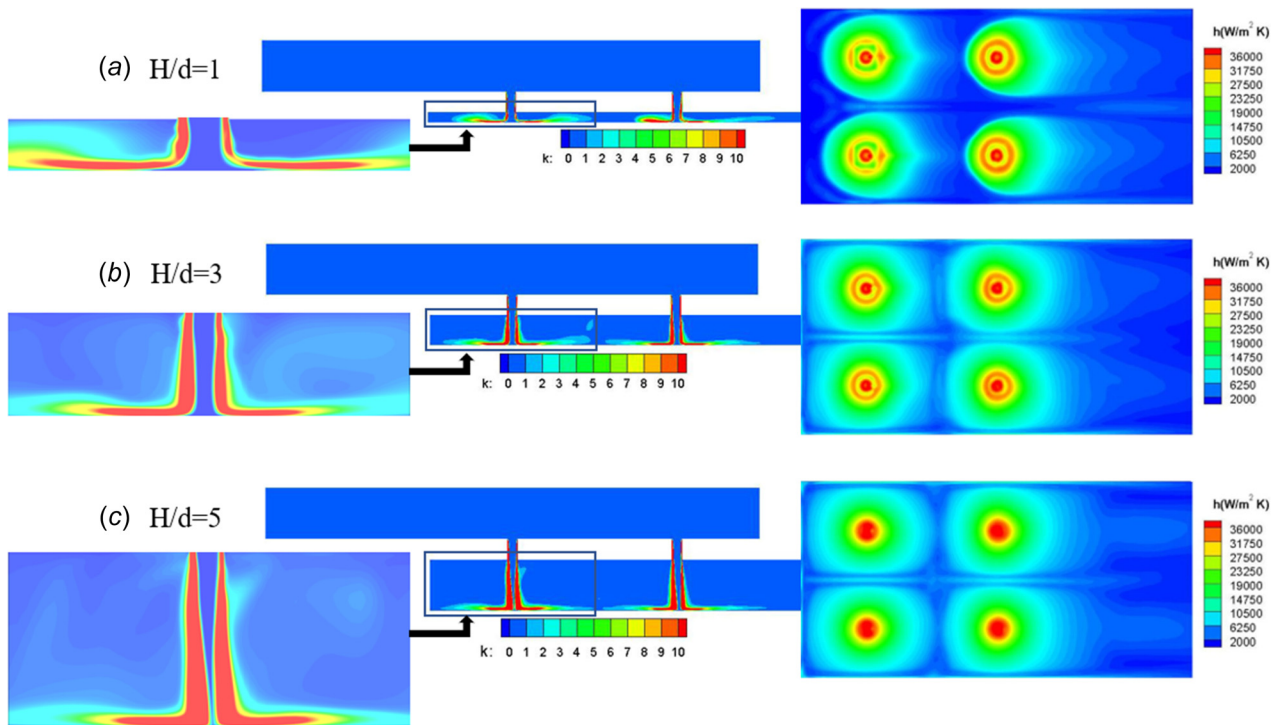

Fig. 5 The heat transfer coefficients on the target plate and the turbulent kinetic energy of the jet flow for different separation distances

as shown in Table 5. There are no vortices between adjacent jets for the small separation distance ($H/d = 1$) because the crossflow is dominant in the flow field. The separation distance $H/d = 3$ gets the best heat transfer uniformity on the target plate. There is nearly no difference of the pressure loss for different separation distances. For separation distance $H/d = 5$, the jets are well developed before reaching the target plate. The turbulent kinetic energy is very high in the core side of the impinging jet and it in the wall region is relatively low. There is nearly no secondary peak of the heat transfer coefficient in the stagnation zone and there are nearly no interferences between adjacent jets for larger separation distance ($H/d = 5$). The shifting of heat transfer peak is obvious with

lower separation distance of $H/d = 1$ and 3. And there is nearly no heat transfer shifting for $H/d = 5$.

5 Conclusions

In the present paper, numerical study of flow and heat transfer properties of RP-3 kerosene in an impingement model are conducted with SST k-ω turbulence model and a 10-species surrogate of kerosene. The heat transfer rates and pressure losses increase with decreasing dimensionless open areas. For the temperature deviation ratio, impingement plate C ($A_f = 0.41\%$) obtains a better uniformity on the target plate. The overall heat transfer performance is better for higher inlet temperature. The separation distance $H/d = 3$ gets the best heat transfer uniformity on the target plate.

Nomenclature

A_f = dimensionless open area
d = diameter of the jets, mm

Table 5 The comparison of heat transfer performance and pressure loss with different separation distances

H/d	Total averaged h (W/m²K)	$\dfrac{\sigma}{\overline{\overline{T}}_w}$	Pressure loss (kPa)
1	10877	32.5%	58
2	12660	8.8%	58
3	12600	7.7%	57
4	12394	7.6%	57
5	12213	7.4%	57

H = separation distance of the impinging jet, mm
h = heat transfer coefficient, W/m^{2}K
k = thermal conductivity, W/mK
L_x/L_y = width and length of the target wall
n = jet number
Q_w = heat flux on the target plate, MW/m^2
Re = Reynolds number
S_x/S_y = distance of the adjacent jets
T_f = inlet temperature, K
T_w = local wall temperature, K
$\bar{T}_w$ = the total averaged temperature on the target plate, K
u = jet velocity, m/s
ρ = density, kg/m^3
σ = local temperature standard deviation, K

References

[1] Hendricks, R. C., Simoneau, R. J., and Smith, R. V., 1970, "Survey of heat transfer to near-critical fluids," NASA Technical Note D-5886.
[2] Bellan, J., 2000, "Supercritical (Subcritical) Fluid Behavior and Modeling: Drops, Streams, Shear and Mixing Layers, and Sprays," Prog. Energy Combust. Sci., 26(4–6), pp. 329–366.
[3] Yang, V., 2000, "Modeling of Supercritical Vaporization, Mixing and Combustion Processes in Liquid-Fueled Propulsion System," Proc. Combust. Inst., 28(1), pp. 925–942.
[4] Linne, D., Meyer, M., Edwards, T., Eitman, D., Linne, D., Meyer, M., Edwards, T., and Eitman, D., 1997, "Evaluation of Heat Transfer and Thermal Stability of Supercritical JP-7 Fuel," AIAA Paper No. 1997-3041.
[5] Hu, Z. H., Chen, T. K., Luo, Y. S., and Zhang, J. X., 2002, "Heat Transfer to Kerosene at Supercritical Pressure in Small-Diameter Tube With Large Heat Flux," J. Chem. Ind. Eng. (China), 53(2), pp. 134–138.
[6] Zhong, F. Q., Fan, X. J., Yu, G., Li, J. G., and Sung, C. J., 2009, "Heat Transfer of Aviation Kerosene at Supercritical Conditions," J. Thermophys. Heat Transfer, 23(3), pp. 543–550.
[7] Dang, G., Zhong, F. Q., Zhang, Y. J., and Zhang, X. Y., 2015, "Numerical Study of Heat Transfer Deterioration of Turbulent Supercritical Kerosene Flow in Heated Circular Tube," Int. J. Heat Mass. Transfer, 85, pp. 1003–1011.
[8] Wang, X., Zhong, F. Q., Chen, L. H., and Zhang, X. Y., 2013, "A Coupled Heat Transfer Analysis With Effects of Catalytic Cracking of Kerosene for Actively Cooled Supersonic Combustor," J. Propul. Technol., 34(1), pp. 47–53.
[9] Buchlin, J. M., 2003, "Convective Heat Transfer in Impinging Gas-Jet Systems," (Lecture Series 2000–03), von Karman Institute for Fluid Dynamics,Rhode Saint Genese, Belgium, pp. 1–33.
[10] Han, B., and Goldstein, R., 2003, "Aero-Thermal Performance of Internal Cooling Systems in Turbomachines," (Lecture Series 2000–03), von Karman Institute for Fluid Dynamics, Rhode Saint Genese, Belgium, pp. 34–57.
[11] Chambers, A., Gillespie, D., Ireland, P., and Mitchell, M., 2006, "Enhancement of Impingement Cooling in a High Cross Flow Channel Using Shaped Impingement Cooling Holes," ASME Paper No. GT2006-91229.
[12] Son, C., Gillespie, D., Ireland, P., and Dailey, G., 2001, "Heat Transfer and Flow Characteristics of an Engine Representative Impingement Cooling System," J. Turbomach., 123(1), pp. 154–160.
[13] Xing, Y. F., Zhong, F. Q., and Zhang, X. Y., 2018, "Numerical Study of Impingement Cooling of Aviation Kerosene at Supercritical Conditions," ASME J. Heat Transfer-Trans. ASME, 140(11), p. 112201.
[14] Zu, Y. Q., and Yan, Y. Y., 2009, "Numerical Study on Stagnation Point Heat Transfer by Jet Impingement in a Confined Narrow Gap," ASME J. Heat Transfer-Trans. ASME, 131(9), p. 094504.
[15] Sagot, B., Antonini, G., Christgen, A., and Buron, F., 2008, "Jet Impingement Heat Transfer on a Flat Plate at a Constant Wall Temperature," Int. J. Therm. Sci., 47(12), pp. 1610–1619.
[16] Cheng, L., Zhong, F., Gu, H., and Zhang, X., 2016, "Application of Conjugate Gradient Method for Estimation of the Wall Heat Flux of a Supersonic Combustor," Int. J. Heat Mass. Transfer, 96, pp. 249–255.
[17] "Examining Spatial (Grid) Convergence," accessed Apr. 12, 2022, www.grc.nasa.gov/www/wind/valid/tutorial/spatconv.html
[18] Du, M. M., Zhong, F. Q., Xing, Y. F., and Zhang, X. Y., 2020, "Experimental and Numerical Investigation on Flow and Heat Transfer of Impingement Jet Cooling of Kerosene," Int. Commun. Heat Mass Transfer, 116, p. 104644.
[19] Choo, K. S., Youn, Y. J., Kim, S. J., and Lee, D. H., 2009, "Heat Transfer Characteristics of a Micro-Scale Impinging Slot Jet," Int. J. Heat Mass. Transfer, 52(13–14), pp. 3169–3175.
[20] Pence, D. V., Boeschoten, P. A., and Liburdy, J. A., 2003, "Simulation of Compressible Micro-Scale Jet Impingement Heat Transfer," ASME J. Heat Transfer-Trans. ASME, 125(3), pp. 447–453.